Send Orders for Reprints to reprints@benthamscience.net

International Journal of Sensors, Wireless Communications and Control, **2020,** *10,* **00-00**

RESEARCH ARTICLE

Photonic Crystal Based Bio-Sensor Detection in Nanophotonic Structure Using FEM Method

Mehdi Ghoumazi[1,2,*] and Abdesselam Hocini[1]

[1]*Laboratoire d'Analyse des Signaux et Systèmes, Université de M'sila, M'sila 28000, Algeria;* [2]*Unité de Recherche en Optique et Photonique (UROP-Sétif), Centre de Développement des Technologies Avancées (CDTA), Cité 20 Aout 1956 Baba Hassen, Algiers, Algeria*

ARTICLE HISTORY

Received: May 22, 2019
Revised: August 20, 2019
Accepted: October 15, 2019

DOI:
10.2174/2210327910666191218125109

Abstract: ***Background & Objective*****:** In this article, a nano-cell coupled 2D photonic crystal waveguide bio- detection platform is proposed for the detection of organic liquids such as water, ethanol, glycerol, benzene and bromine for different refractive indices (n). The detection characteristics are analyzed and obtained for the band diagram, before and after change of radius (r) as well as after the injection of liquids into the heart of the nanostructure cell at the resonant wavelength (λ res). Also, we extracted variations from the power flow norm (P) to the resonance and the transmission (T) for each material. This nanostructure for different (n) materials used, gives (P) at different levels to the resonance. This explains the importance of the refractive index parameter (n) which plays a crucial role in the detection of materials.

Conclusion**:** The proposed biosensor enables the detection of liquids. This is shown through the numerical results obtained. These results give a good observation of the different behavior of the signal in the presence of the liquids used which depend on their refractive indices 'n'. This parameter 'n' is very important for detection when it varies from material to material. The proposed biosensor can be used in several research areas, particularly in medical and environmental applications.

Keywords: Photonic crystals, finite element method (FEM), photonic sensor, organic liquids.

1. INTRODUCTION

Optical biosensors have attracted much attention in recent times [1]. They are many powerful detection and analysis tools that have many applications in the healthcare, pharmaceutical industry, environmental monitoring, and food processing industries. A lot of detection techniques do not easily adapt to the planar lab on chip type systems because of their requirement of a large sensing area of the order of mm^2 [2, 3].

Moreover, photonic crystals (PhCs) constitute a new research direction in the field of optical sensing. PhCs are nano-sized periodic dielectric structures and devices with a refractive index that is modulated with the wavelength-scale periodicity in one two and three dimensions [4, 5, 6, 7]. This periodicity results in a wavelength region in which the propagation of optical waves is prohibited. This wavelength region is called the photonic bandgap (PBG) [8]. Due to the remarkable importance of PBG, many applications of PhCs depend on their PBG's proprieties [9, 10]. Different optical devices based on PhC can be developed by creating appropriate defects. Various optical devices can be realized based on PhC such as splitters [11], logic gates [12], polarizers [13], triplexer [14], optical power dividers [15], optical waveguides [16], bandstop filters [17], optical converters [18], and optical sensors [19, 20]. We remove some rods or holes inside the PhC structure in order to obtain a ring or cavity shape.

In this article, two-dimension photonic crystals are used due to their simplicity in shape and small size as well as the high confinement of light inside the device, which gives them a well- defined and accurate sensing platform [21].

Photonic Crystals (PhCs) as well as circular ring photonic crystals (PhCRR) based on sensors have been used for biosensing applications [22], chemical sensors [23], temperature sensors [24], cancer sensing [25], etc.

In this work, we designed a biosensor based photonic crystal. We represented sensing characteristics such as the

*Address correspondence to this author at the Laboratoire d'Analyse des Signaux et Systèmes, Université de M'sila, M'sila 28000, Algeria; Unité de Recherche en Optique et Photonique (UROP-Sétif), Centre de Développement des Technologies Avancées (CDTA), Cité 20 Aout 1956 Baba Hassen, Algiers, Algeria; E-mail: mehdi.ghoumazi@univ-msila.dz

2210-3279/20 $65.00+.00

propagation at resonant wavelength before and after changing parameters (such as the radius of photonic crystals), the power flow norm and transmission for water, ethanol, glycerol, benzene and bromine. MATLAB and COMSOL simulators are used to draw the band diagram, and determine the power flow and the transmission for the sensor.

2. DESIGN PROCEDURE

2.1. Structure Design Before Changing Rods

Plane-wave expansion method (PWE) and finite-element (FEM) numerical methods have been used to obtain the photonic bandgap (PBG). Propagation, power flow norm and transmission for different organic liquids in structure were extracted using COMSOL software. We used the proposed photonic crystal-based liquid sensor to detect water, ethanol, glycerol, benzene and bromine. The biosensor, as shown in Fig. (**1**), was designed by using a two-dimensional photonic crystal (PhC) composed of 19X23 square lattice of dielectric rods immersed in the air with lattice constant a=523nm. The refractive index of the rods (Si) is 3.46 and for the air background, it is 1. The radius of rods of perfect PhC (with no defects) is 'r=0.19*a' which is 99.37nm.

Firstly, we created a waveguide by removing some rods in the Γ-X direction and cell shape inside the two-dimensional PhC by removing some rods. Photonic crystals control the light propagation inside the structure with the help of the defect line; that defect can be used for sensing applications [26].

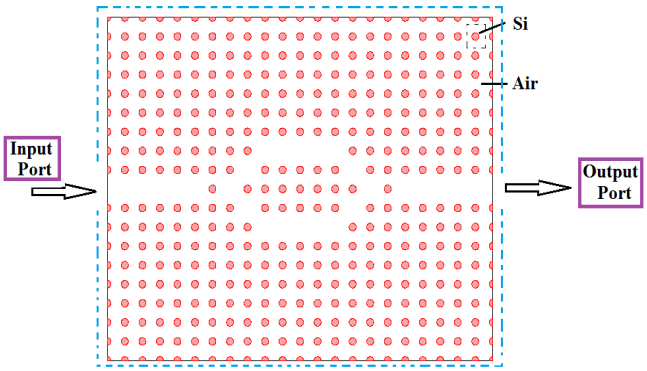

Fig. (1). The initial proposed structure without changed rods. *(A higher resolution / colour version of this figure is available in the electronic copy of the article).*

By introducing some defects inside the structure, the PBG is broken; this allows the guided modes to propagate inside the PBG region. The defects (point/line) are used to design the proposed sensor. The guided modes are regulated by controlling the defect shape and size [27].

Fig. (**2**). displays three PBGs for TM mode (yellow zone).The first TM PBGs range of wavelength 'λ' is [1215.99, 1809.68]nm, the second TM PBGs of wavelength 'λ' is [693.206, 725.28] nm and the third TM PBGs wavelength 'λ' is [577.83, 594.99] nm, knowing that the PBGs are large, medium and narrow, respectively. Only the first PBG in TM mode is large enough for covering the sufficient wavelengths for optical communication applications. In order to have maximum compatibility with optical communication ranges, we took a= 523nm, where the wavelength will be in the range of 1215.99nm<λ<1809.68nm in TM mode.

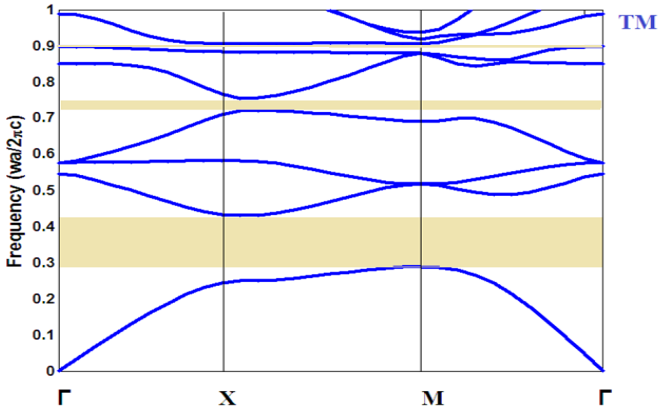

Fig. (2). The band structure for TM mode of the proposed structure. *(A higher resolution / colour version of this figure is available in the electronic copy of the article).*

As explained above, to realize the proposed sensor in a fundamental platform, we first removed a row of dielectric rods from the middle of the structure at the Γ-X direction in order to have an input and output port. Secondly, we removed some rods from the 11 X 7 arrays of dielectric rods at the appropriate place for creating a cell shape. The radius of the cell form is the same as the radius of all other rods in the initial PhC structure (Fig. **1**). Then, we changed the radius of some rods in the heart of the cell for a new study.

Figs. (**3** and **4**) represent the refractive index distribution along the proposed initial structure and the mesh that goes with it.

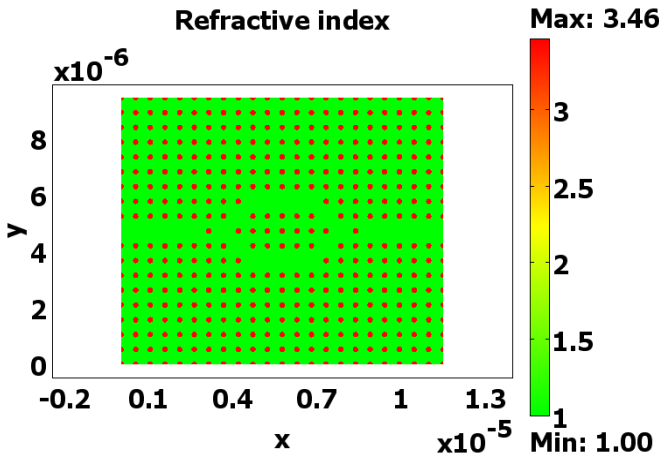

Fig. (3). The distribution of the refractive index in the proposed structure. *(A higher resolution / colour version of this figure is available in the electronic copy of the article).*

Fig. (**5a** and **5b**) represent the electric field distribution of the proposed structure at Resonance, λ =1.39758 μm and at λ =1.3974 μm.

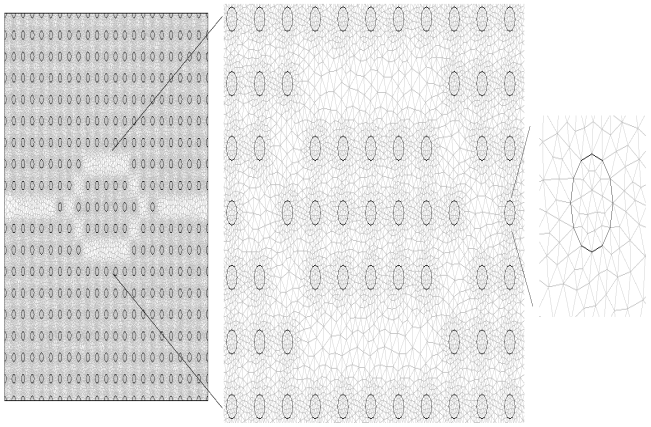

Fig. (4). The proposed structure with fine mesh.

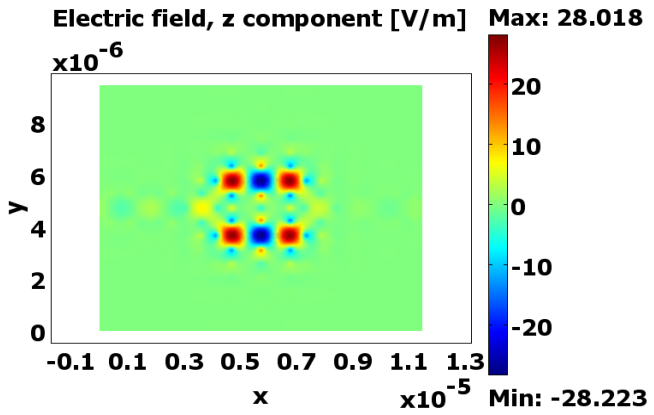

Fig. (5a). The electric field distribution of the proposed structure at Resonance, λ =1.39758 μm. *(A higher resolution / colour version of this figure is available in the electronic copy of the article).*

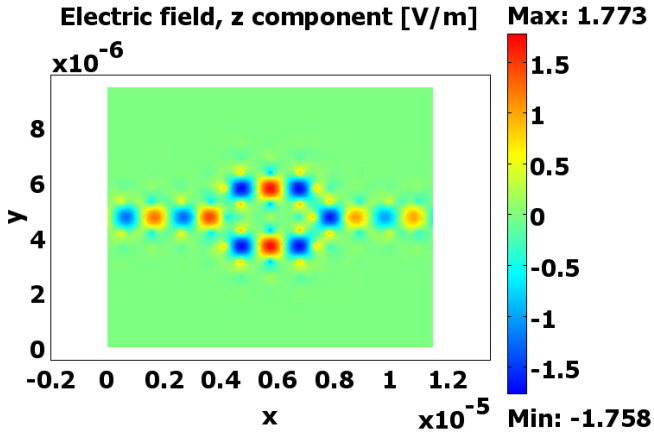

Fig. (5b). The electric field distribution of the proposed structure at λ =1.3974 μm. *(A higher resolution / colour version of this figure is available in the electronic copy of the article).*

2.2. Structure Design After Changing Rods

In the next section, we changed the radius of some rods in the structure's cell shape as depicted in Fig. (**6**).

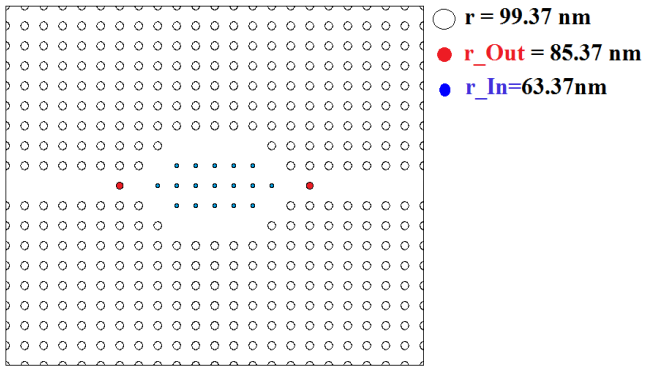

Fig. (6). The initial proposed structure with changed rods. *(A higher resolution / colour version of this figure is available in the electronic copy of the article).*

Figs. (**7** and **8**) illustrate the distribution of the refractive index of the proposed structure and its fine mesh associated with a small change on some rays inside and outside the cell where r_In = 63.37nm (blue color) and r_Out = 85.37nm (red color).

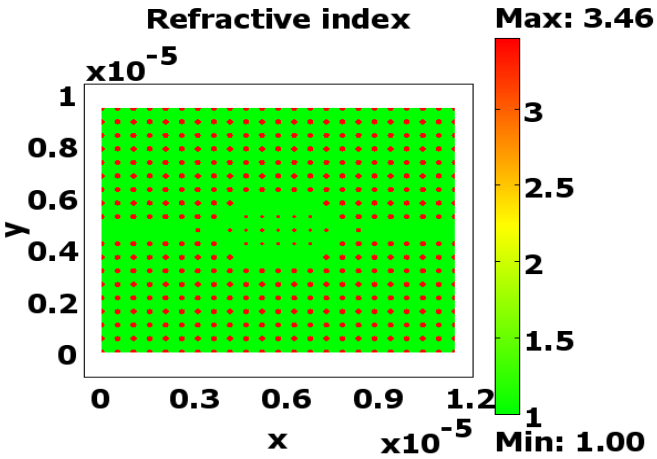

Fig. (7). The distribution of the refractive index in the proposed structure after change rods. *(A higher resolution / colour version of this figure is available in the electronic copy of the article).*

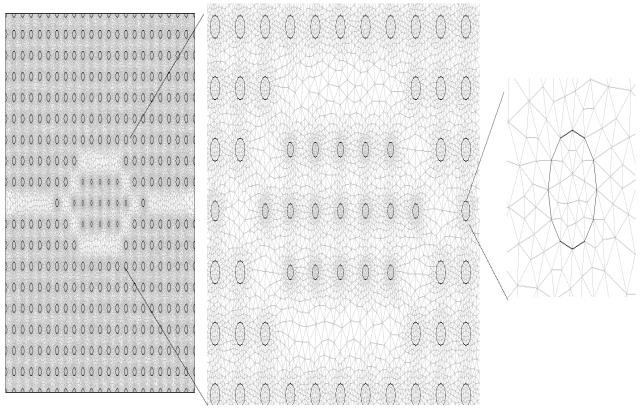

Fig. (8). The proposed structure after changed rods with fine mesh

Fig. (**9**). displays the electric field distribution along the structure at resonance wavelength, λ=1.55μm.

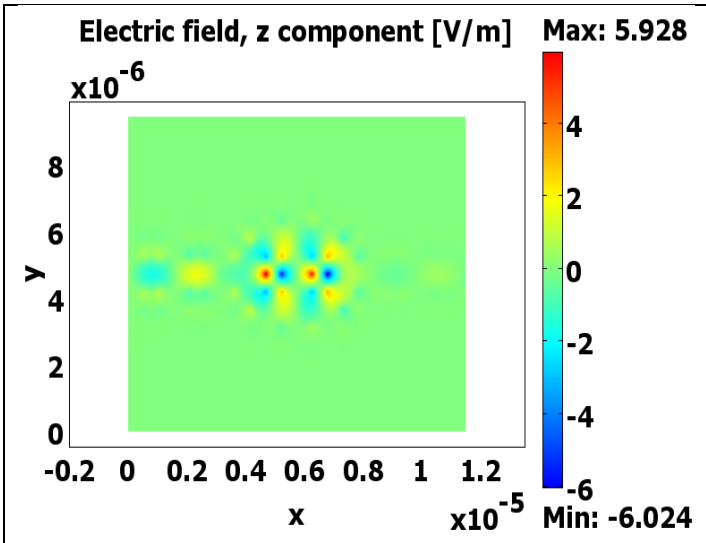

Fig. (9). The electric field distribution of the proposed structure at resonance wavelength λ=1.55µm. *(A higher resolution / colour version of this figure is available in the electronic copy of the article).*

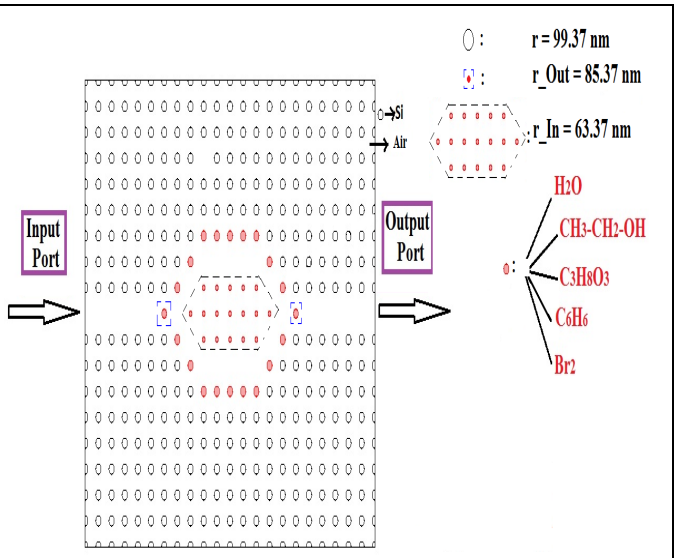

Fig. (10). The final proposed structure (sensor) after changed rods. *(A higher resolution / colour version of this figure is available in the electronic copy of the article).*

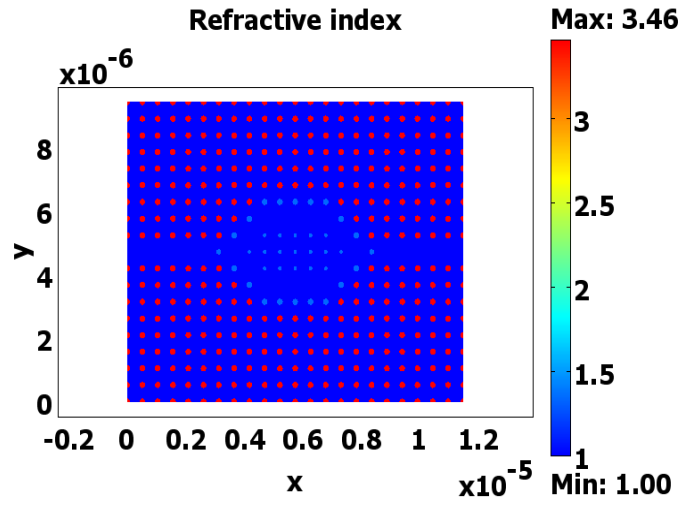

Fig. (11). The distribution of the refractive index in the sensor. *(A higher resolution / colour version of this figure is available in the electronic copy of the article).*

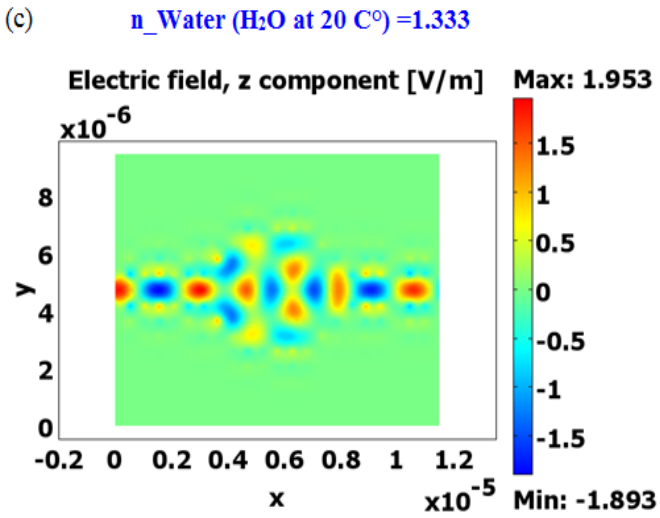

Fig. (12c). The electric field distribution of the proposed sensor for water at resonance wavelength, λ= 1.55µm. *(A higher resolution / colour version of this figure is available in the electronic copy of the article).*

3. BIOSENSOR DESIGN AND SIMULATION

From Fig. (**10**), the final proposed structure (sensor) after changing the radius of some of the rods is represented by two waveguides and a cell resonator. The straight waveguide is created by introducing a defect line and a cell resonator by creating defects point and defects line. The radii of the inner rod and outer rod are 63.37nm and 85.37 nm, respectively. The proposed sensor overall size is 119.53µm^2

So, Fig. (**11**) shows the refractive index distribution along the sensor and Fig. (**12c, 12d, 12e, 12f, and 12g**) show the electric field distribution after the change of the radius for different liquids such as, (c) water, (d) ethanol, (e) glycerol, (f) benzene and (g) bromine at resonance wavelength, λ= 1.55µm.

Also, Fig. (**13h**, **13i**, **13j**, **13k** and **13l**) show the power flow norm going from port 1 to port 2 through the cell shape for different liquids namely, (h) water, (i) ethanol, (j) glycerol, (k) benzene and (l) bromine, respectively at resonance wavelength λ= 1.55µm depending on the cross-section line.

4. DISCUSSION OF BIOSENSOR RESULTS

The numerical results are obtained from the finite element method (FEM) using the COMSOL software [28]. In the first section, we first presented and studied a two-dimensional square lattice nanostructure based on silicon-based (Si) photonic crystals in the air. At the heart of this structure is a cell shape wedged between two waveguides in

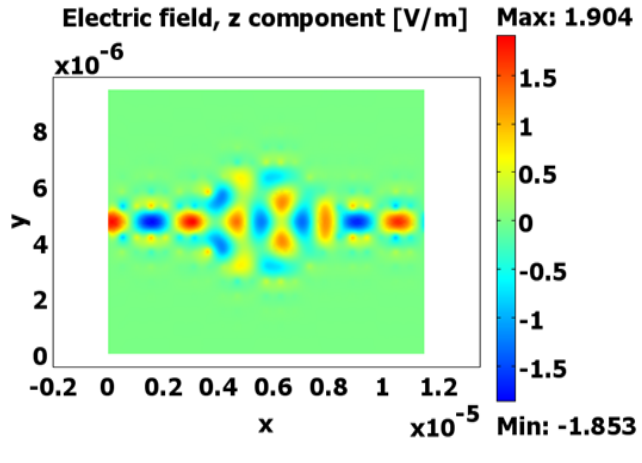

Fig. (12d). The electric field distribution of the proposed sensor for Ethanol at resonance wavelength, λ= 1.55µm. *(A higher resolution / colour version of this figure is available in the electronic copy of the article).*

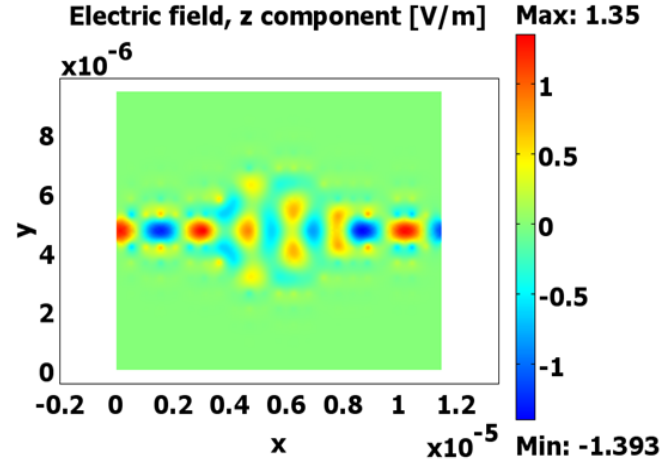

Fig. (12e). The electric field distribution of the proposed sensor for Glycerol at resonance wavelength, λ= 1.55µm. *(A higher resolution / colour version of this figure is available in the electronic copy of the article).*

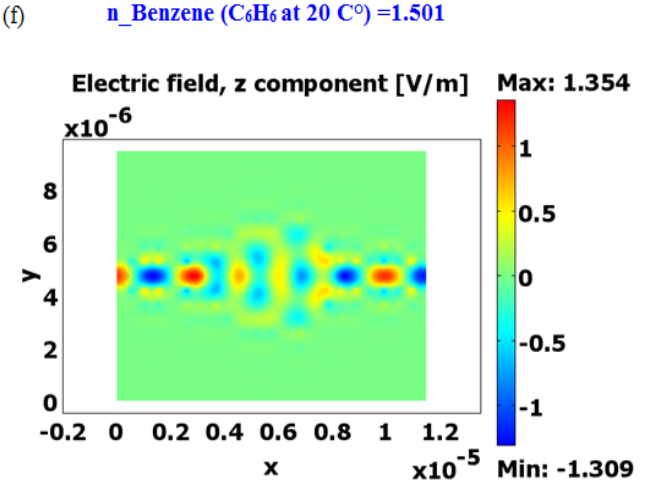

Fig. (12f). The electric field distribution of the proposed sensor for Benzene at resonance wavelength, λ= 1.55µm. *(A higher resolution / colour version of this figure is available in the electronic copy of the article).*

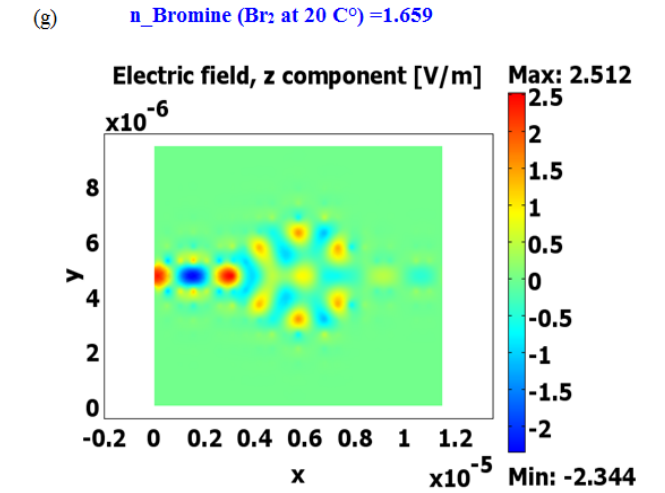

Fig. (12g). The electric field distribution of the proposed sensor for Bromine at resonance wavelength, λ= 1.55µm. *(A higher resolution / colour version of this figure is available in the electronic copy of the article).*

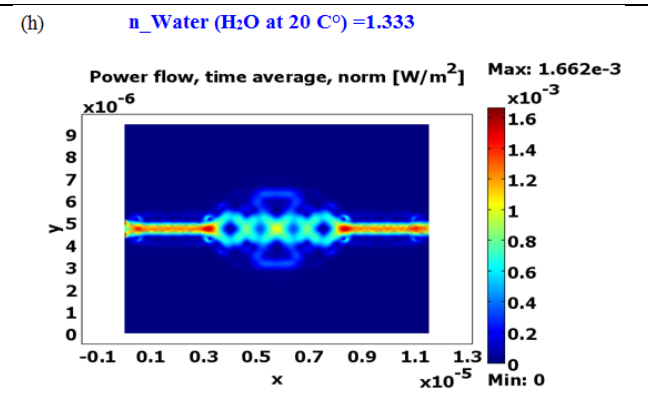

Fig. (13h). The power flow norm distribution of the proposed sensor for water at λ= 1.55µm depending on the cross-section line. *(A higher resolution / colour version of this figure is available in the electronic copy of the article).*

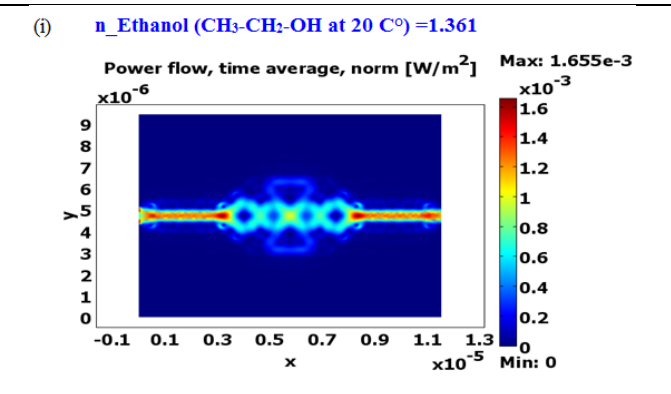

Fig. (13i). The power flow norm distribution of the proposed sensor for ethanol at λ= 1.55µm depending on the cross-section line. *(A higher resolution / colour version of this figure is available in the electronic copy of the article).*

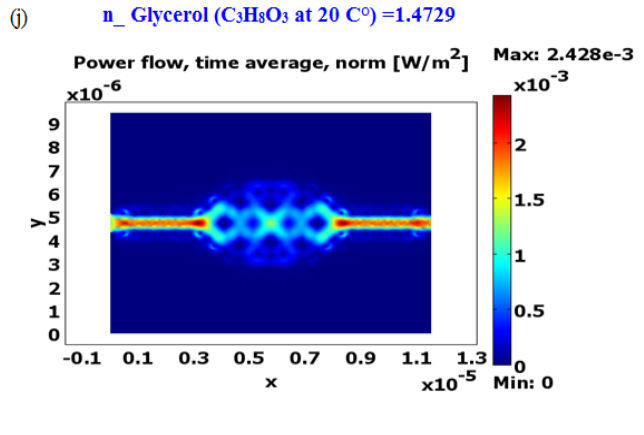

Fig. (13j). The power flow norm distribution of the proposed sensor for Glycerol at λ= 1.55µm depending on the cross-section line. *(A higher resolution / colour version of this figure is available in the electronic copy of the article).*

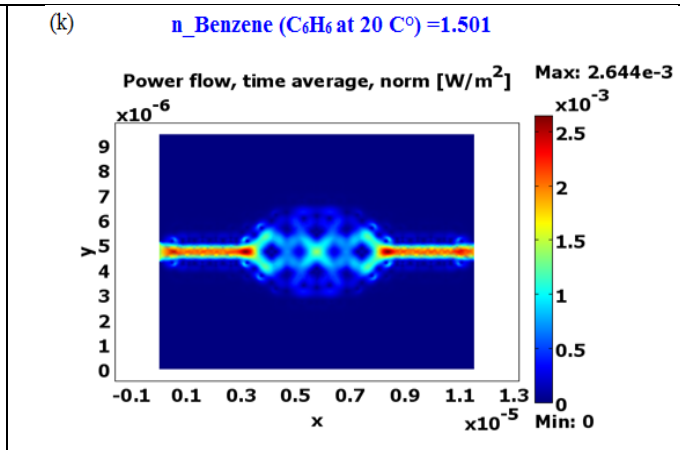

Fig. (13k). The power flow norm distribution of the proposed sensor for Benzene at λ= 1.55µm depending on the cross-section line. *(A higher resolution / colour version of this figure is available in the electronic copy of the article).*

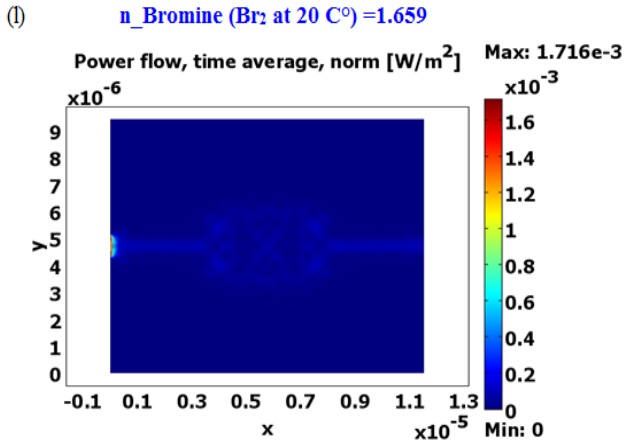

Fig. (13l). The power flow norm distribution of the proposed sensor for Bromine at λ= 1.55µm depending on the cross-section line. *(A higher resolution / colour version of this figure is available in the electronic copy of the article).*

the Γ-M direction. The radius (r) of the rod is the same in the whole structure, which is 93.37nm and the lattice constant "a" is 493nm.

Figs. (**3-5**) show the distribution of the refractive index and the fine mesh along the proposed structure before changing the radius (r) at the heart of the resonator cell as well as the distribution of the electric field at different wavelengths (Fig. **5a** at resonance λ=1,39758µm and Fig. (**5b**) at non resonance, λ=1,3974µm). Whereas, in Figure.6, the same previous results are presented but with a change in the radius of the resonator cell (see Fig. **7-9**) at λ=1.55µm.

Subsequently, the study of our bio-sensor focused on the base of the structure shown in Fig. (**6**) by injecting liquids inside the cell (see Fig. **10**) such as, water (H_2O), ethanol (CH_3-CH_2 -OH), glycerol ($C_3H_8O_3$), benzene (C_6H_6) and bromine (Br_2), which have the following refractive indices: 1.333, 1.361, 1.4729, 1.501 and 1.659, respectively at λ = 1.55µm. On the one hand, the result obtained, such as the distribution of the refractive index of the sensor is shown in Fig. (**11**) and for the different injected liquids, the results are depicted in Fig. (**12c**, **12d**, **12e**, **12f** and **12g**), which show the electric field distribution at the resonant wavelength. On the other hand, Fig. (**13h**, **13i**, **13j**, **13k** and **13l**) represent a clear picture of the power flow norm from port 1 to port 2 through the resonator cell for the different liquids used previously.

Fig. (**14**) summarizes the results of Figs. (**13**) which is a comparison of the degree of biosensor power flow norm behavior with the presence of the liquids used as a function of the cross-section line.

In Fig. (**14**), it can be observed that the benzene (Br_2) of n=1.501 reaches the highest power at 9.41nW/m^2 (magenta color) followed by water (cyan color) and glycerol (green color) with the refraction index 1.333 and 1.4729 for maximum values: 9.1nW/m^2 and 8.97nW/m^2, respectively. After that, ethanol (black color), which has a refractive index of 1.361, manifests itself with a considerable maximum equal to 8.25nW/m^2. In addition, low power of 0.4923nW/m^2 is observed at the level of bromine (blue color) which has a refractive index of 1.659. Finally, we also represented on the

same graph a curve (red color) before the injection of organic liquids in the cell, which is the refractive index of silicon is 3.46. It is observed that the power before the injection of its liquids is almost non-existent. In this case, it can be said that the power could reach different maximums along the path from port 1 to port 2 in the presence of the organic liquids used. Knowing that these maximums intersect in the same cross-sectional line at 5.754 µm.

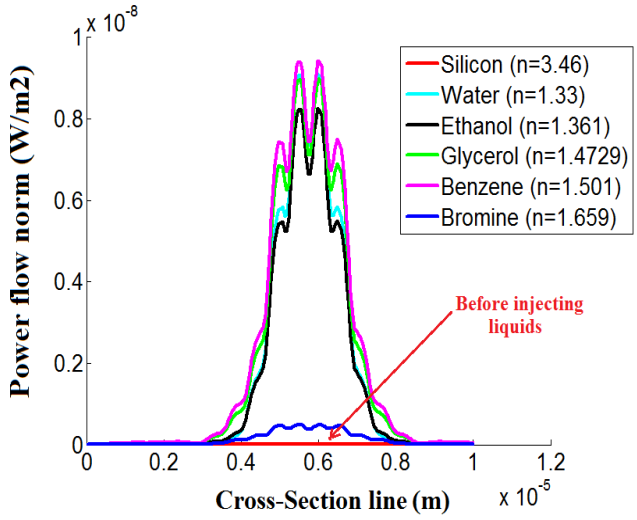

Fig. (14). The power flow norm distribution of: Water (H_2O), ethanol (Ch_3-Ch_2-OH), glycerol ($C_3H_8O_3$), benzene (C_6H_6) and bromine (Br_2) versus Cross-Section line. *(A higher resolution / colour version of this figure is available in the electronic copy of the article).*

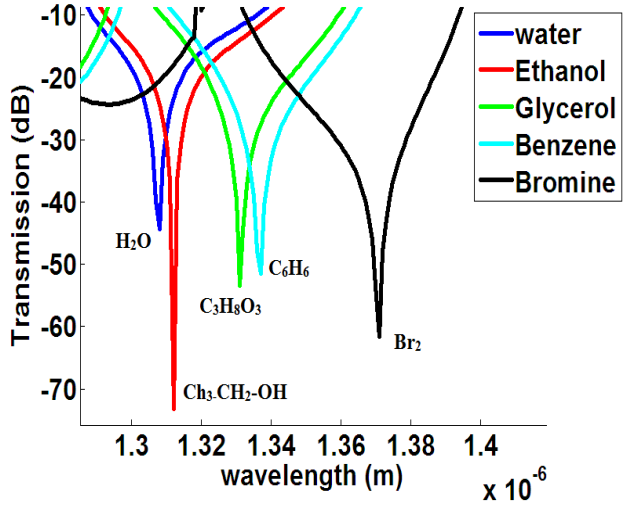

Fig. (15). Transmission for water (H_2O), Ethanol (CH_3-CH_2-OH), glycerol ($C_3H_8O_3$), benzene (C_6H_6), bromine (Br_2) versus wavelength. *(A higher resolution / colour version of this figure is available in the electronic copy of the article).*

From Fig. (**15**), the transmission in dB of the structure is represented depending on wavelength. We can see that for the different materials used, the transmission coefficient passes through maximums.

In the case of benzene (C_6H_6), it is clear that the transmission coefficient reaches a value of -51.93dB for a wavelength λ = 1.337µm, for water (H_2O), it is 44.29dB at a wavelength of 1.308 µm and for glycerol ($C_3H_8O_3$), the transmission coefficient reaches a value of -53.41 dB at the wavelength λ = 1.331 µm. For the last two materials, ethanol (CH_3-CH_2-OH) transmission coefficient reaches a value of -73.22dB at λ = 1.312µm and bromine (Br_2) transmission coefficient is -61.56dB at a wavelength equal to 1.371 µm. This difference in transmission coefficient and wavelength is due to the refractive index which varies with respect to each material.

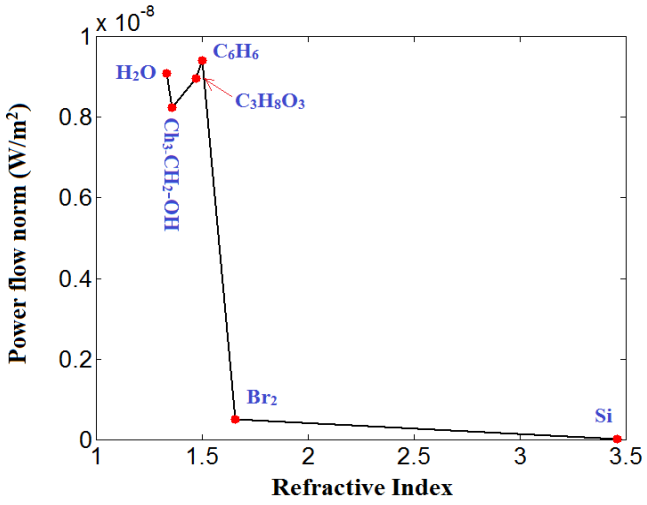

Fig. (16). The power flow norm versus the refractive index of: Water (H_2O), Ethanol (CH_3-CH_2–OH), glycerol ($C_3H_8O_3$), benzene (C_6H_6), bromine (Br_2) and Silicon (Si). *(A higher resolution / colour version of this figure is available in the electronic copy of the article).*

Fig. (**16**) depicts the variation in the power flow norm in the function of the refractive index of all the materials used in this study. It was observed that benzene (C_6H_6) reached a high power followed by water (H_2O) and glycerol ($C_3H_8O_3$). Then, ethanol (CH_3-CH_2-OH) was also expressed with considerable power. In addition, the bromine (Br_2) reached a low power and finally in the absence of liquids in the cell, the power is almost non-existent as in the case of silicon (initial state). These power variations are due to the variation in the refractive index of each organic material used and the behavior it shows.

CONCLUSION

In this paper, we = proposed a biosensor based on photonic crystals in order to detect certain liquids, namely water, ethanol, glycerol, benzene, and bromine. The biosensor consists of a nanostructure composed of a resonator cell between two waveguides that are on the same line. This biosensor is designed using two-dimensional photonic crystals with a square array of rods embedded in the air. The range in which the biosensor operates is from 1215.99nm to 1809.68nm. The surface of the biosensor is 11.506nm x 9.414nm ≈108nm^2. The numerical results of the propagation and the

power flow norm obtained by COMSOL facilitate good observation of the different behaviors of the signal in the presence of the liquids used, which depend on their refractive indices 'n'. The parameter ‘n’ is very important in terms of detection when it varies from one material to another. The proposed biosensor can be used in several fields of research, particularly, medical and environmental applications.

AVAILABILITY OF DATA AND MATERIAL

Not applicable

FUNDING ALONG WITH GRANT NUMBER

Not applicable

ETHICS APPROVAL AND CONSENT TO PARTICIPATE

Not applicable.

HUMAN AND ANIMAL RIGHTS

No Animals/Humans were used in the study that is the basis of this research.

CONSENT FOR PUBLICATION

Not applicable.

CONFLICT OF INTEREST

The authors declare no conflict of interest, financial or otherwise.

ACKNOWLEDGEMENTS

Declared none.

REFERENCES

[1] Li B, Lan D, Zhang Z. Chemiluminescence flow-through biosensor for glucose with eggshell membrane as enzyme immobilization platform. Anal Biochem 2008; 374(1): 64-70. [http://dx.doi.org/10.1016/j.ab.2007.10.036] [PMID: 18036547]

[2] Fan X, White IM, Shopova SI, Zhu H, Suter JD, Sun Y. Sensitive optical biosensors for unlabeled targets: a review. Anal Chim Acta 2008; 620(1-2): 8-26. [http://dx.doi.org/10.1016/j.aca.2008.05.022] [PMID: 18558119]

[3] Dorfner D, Zabel T, Hürlimann T, *et al.* Photonic crystal nanostructures for optical biosensing applications. Biosens Bioelectron 2009; 24(12): 3688-92. [http://dx.doi.org/10.1016/j.bios.2009.05.014] [PMID: 19501502]

[4] Abbaspour A, Alipour-Banaei H, Andalib A. The new method for Optical Channel Drop Filter with High Quality Factor Based on Triangular Photonic Crystal Design. Journal of Articficial Intelligence in Electreical Engineering 2013; 2(6)

[5] Zouache T, Hocini A, Harhouz A, Mokhtari R. Design of pressure sensor based on two-dimensional photonic crystal. Acta Phys Pol A 2017; 131(1): 68-70. [http://dx.doi.org/10.12693/APhysPolA.131.68]

[6] Zhang D, Jia H. Numerical Analyses of Leaky Modes in Two-Dimentional Photonic Crystal Waveguides Using Fourier Series Expansion Method with Perfectly Matched Layer. IEICE Trans Electron 2007; E90-C(3): 613-22. [http://dx.doi.org/10.1093/ietele/e90-c.3.613]

[7] Benjeloul R, Bouchemat T, Bouchemat M. An optical channel drop filter based on 2D photonic crystal ring resonator. J Electromagn Waves Appl 2016; V30: 2402-10. [http://dx.doi.org/10.1080/09205071.2016.1253508]

[8] Hocini A, Moukhtari R. Khedrouche, Kahlouche A, Zamani M. Magneto-photonic crystal microcavities based on magnetic nanoparticles embedded in Silica matrix. Opt Commun 2017; 384: 111-7. [http://dx.doi.org/10.1016/j.optcom.2016.10.020]

[9] Joannopoulos JD, Johnson SG, Winn JN, Meade RD. Photonic Crystals: Molding the Flow of Light Princeton (NY): Princeton University Press. 2008; p. 304.

[10] Zamani M, Hocini A. Large Faraday rotation in magnetophotonic crystals containing SiO2/ZrO2 matrix doped with CoFe2O4 magnetic nanoparticles. Opt Mater 2016; (56): 306-9. [http://dx.doi.org/10.1016/j.optmat.2016.05.062]

[11] Ghafari A, Monifi F, Djavid M, Abrishamian MS. J Appl Sci (Faisalabad) 2008; (8): 14-6.

[12] Fasihi K. High-contrast all-optical controllable switching and routing in nonlinear photonic crystals. J Lightwave Technol 2014; 32(18): 3126-31. [http://dx.doi.org/10.1109/JLT.2014.2334613]

[13] Zabelin V, Dunbar LA, Le Thomas N, *et al.* Self-collimating photonic crystal polarization beam splitter. Opt Lett 2007; 32(5): 530-2. [http://dx.doi.org/10.1364/OL.32.000530] [PMID: 17392911]

[14] Labbani A, Benghalia A. Design of photonic crystal triplexer with core-shell rod defects. Chin Phys Lett 2015; 32(5): 63-5. [http://dx.doi.org/10.1088/0256-307X/32/5/054204]

[15] Mesri N, Alipour-Banaei H. An optical power divider based on twodimensional photonic crystal structure. Journal of Optical Communications 2017; 38(2): 129-32. [http://dx.doi.org/10.1515/joc-2016-0069]

[16] Janrao N, Zafar R, Janyani V. Improved design of photonic crystal waveguides with elliptical holes for enhanced slow light performance. Optical engineering 2012; 51(6)064001. : 1-7. [http://dx.doi.org/10.1117/1.OE.51.6.064001]

[17] Monifi F, Djavid M, Ghafari A, Abrishamian MS. A New Bandstop Filter based on Photonic Crystals. Propgress In Electromagnetics Research Symposium, Comridge. 674-6.

[18] Mehdizadeh F, Soroosh M, Alipour-Banaei H, Farshidi E. A Novel Proposal for All Optical Analog-to-Digital Converter Based on Photonic Crystal Structures. IEEE Photonics J 2017; 9(2): 1-11. [http://dx.doi.org/10.1109/JPHOT.2017.2690362]

[19] Zouache T, Hocini A, Wang X. Cavity-coupled photonic crystal waveguide as highly sensitive platform for pressure sensing. Optik (Stuttg) 2018; 172: 97-106. [http://dx.doi.org/10.1016/j.ijleo.2018.06.120]

[20] Hocini A, Harhouz A. Modeling and analysis of the temperature sensitivity in two dimensional photonic crystal microcavity. J Nanophotonics 2016; 10(1)016007 [http://dx.doi.org/10.1117/1.JNP.10.016007]

[21] Lee MR, Fauchet PM. Two-dimensional silicon photonic crystal based biosensing platform for protein detection. Opt Express 2007; 15(8): 4530-5. [http://dx.doi.org/10.1364/OE.15.004530] [PMID: 19532700]

[22] Olyaee S, Bahabady AM. Designing a novel photonic crystal nanoring resonator for biosensor application. Opt Quantum Electron 2014; 53(6): 1881-8.

[23] Hsiao FL, Lee C. Computational study of photonic crystal nanoring resonator for biomedical sensing. IEEE Sens J 2010; 10(7): 1185-91. [http://dx.doi.org/10.1109/JSEN.2010.2040172]

[24] Radhouene M, Kumar Chhipa M, Nadjar M, Robinson S. Suthar B. Novel Design of Ring Resonator Based Temperature Sensor Using Photonics TechnologyPhonic sensors 2017; 7: 311-6.

[25] Jindal S, Sobti S, Kumar M, Sharma S, Kumar Pal M. Nanocavity-coupled Photonic Crystal Waveguide as Highly Sensitive Platform for cancer Detection IEEE sensors Journals 2016; 6(10): 3705-10.

[26] Joannopoulos JD, Villeneuve PR, Fan S. Photonic crystals: putting a new twist on light. Nature 1997; 386(6621): 143-9. [http://dx.doi.org/10.1038/386143a0]

[27] Robinson S, Dhanlaksmi N. Photonic Crystal Based Biosensor for the Detection of Glucose Concentration in Urine. Photonic Sens 2016; 7(1): 11-9. [http://dx.doi.org/10.1007/s13320-016-0347-3]

[28] www.comsol.com